

# Analysis of Resolution as a Function of Microparticle Size in Virtual Super-Resolution Optical Imaging for 2D System

A. R. Bekirov, N. A. Lysceva, B. S. Luk'yanchuk, and A. A. Fedyanin  
*Lomonosov Moscow State University*  
[bekirov@nanolab.phys.msu.ru](mailto:bekirov@nanolab.phys.msu.ru)

## Abstract

The work shows that visualization using microparticles allows one to distinguish objects that are inaccessible during direct observation. This analysis is based on a full two-dimensional simulation of optical image formation taking into account the diffraction of partially coherent light on the microparticle and the objects under study. The oscillating nature of optical resolution is shown depending on the size of the microparticle. The presence of strong resonances is shown in both transmission and reflection modes.

## 1. Introduction

Various theoretical approaches have been proposed to explain this phenomenon [1-13]. These works are dedicated to modeling the super-resolution effect in virtual imaging facilitated by dielectric microspheres. Among them, some works focus on fully modeling the propagation of radiation from a source through the microsphere to the subsequent image formation [8, 9, 13]. In these models, the objects being imaged are not point dipoles but real structures. Due to computational complexity, such calculations are typically limited to two-dimensional cases. Experimental data confirmed super resolution effect for this case [14]. However, the crucial question of whether a fundamental resolution limit exists remains unresolved. This section examines the minimum achievable resolution in virtual imaging formed by microspheres and its dependence on particle size. Both reflection and transmission geometries are considered.

To investigate this issue, it is practical to use a monochromatic light source. To determine the system's resolution, a series of simulations must be conducted by gradually increasing the distance between the objects, starting from zero, until they become distinguishable in the image. The resolution criterion adopted is based on the Rayleigh criterion: first, the presence of two distinct intensity maxima in the image field; second, the intensity "dip" between the maxima must be 80% of the maximum intensity. It should be noted that some studies relax the second condition, requiring a dip of 95% or more. However, the 80% criterion provides a more reliable estimate of resolution for experimental validation.

In our previous work [13], we proposed a simulation method based on the FDTD (Finite Difference Time Domain) approach, which demonstrated its feasibility. However, this method is computationally intensive. For a monochromatic light source, the FEM (Finite Element Method) is more efficient. While the choice of method is less critical for fixed geometry simulations, the FEM approach becomes significantly advantageous when determining the resolution limit. Therefore, the calculations in this section are performed using the FEM method implemented in the Matlab Partial Differential Equation Toolbox, utilizing the specialized "electromagnetic" class of the "harmonic" type.

The use of the FEM method also enables optimization of the image field calculation geometry, reducing the size of the simulation domain. In this approach, the image field can be computed as diffraction integral [13]:

$$\mathbf{E}^{im}(r_0) = \frac{i}{4} \int_{\Gamma} [G(\mathbf{n}, \nabla) \mathbf{E}^* - \mathbf{E}^*(\mathbf{n}, \nabla) G] dl, \quad (1)$$

where  $\Gamma$  is an arbitrary curve homotopic to an infinite line,  $G = H_0^{(1)}(k|r - r_0|)$  is the Hankel function of the first kind, and  $*$  denotes complex conjugation,  $k=2\pi/\lambda$ ,  $\nabla = \partial / \partial \mathbf{r}$ ,  $\lambda$  is wavelength. The complex conjugation of the source field reverses the wave front, transforming the field from diverging to converging to the source. The curve  $\Gamma$  can be chosen as a hemisphere enclosing the microsphere. Similar optimizations were performed in Ref. [8]. This configuration captures all rays emanating from the microsphere, with the radius of the hemisphere set comparable to the diameter of the microsphere and its center positioned at the contact point between the microsphere and the substrate. If the curve  $\Gamma$  were chosen as a line, achieving the same result would require the line to be significantly larger than the microsphere's diameter, substantially increasing the simulation domain.

## 2. Calculation Setup

For accurate calculations, the mesh size in the source generation and object regions must be especially fine. The maximum distance between mesh nodes was set to  $0.05\lambda$  in the transmission mode and  $0.1\lambda$  in the reflection mode, with further refinement in the specified regions to  $0.005\lambda$ . Simulations were conducted for microsphere sizes  $R=(4:0.05:7)\cdot\lambda$  with a refractive index  $n=1.46$ . In the reflection geometry, the sample consisted of rectangular perfect conductors with a width of  $0.25\cdot\lambda$  and a height of  $0.1\lambda$ . For the transmission geometry, the sample was represented by slits in an opaque screen of the same dimensions. The entire structure was placed on a substrate with a refractive index of  $n=1.46$ . An overview of the calculation setup is shown in Fig. 1.

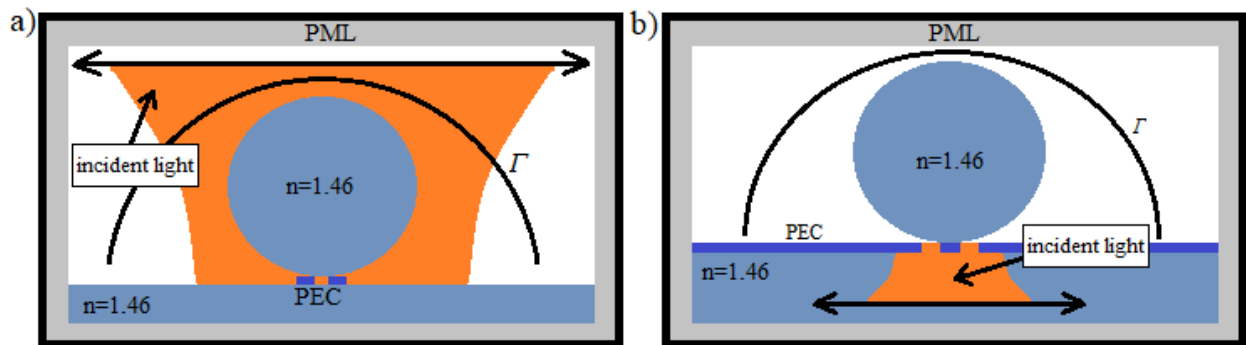


**Fig. 1.** General calculation scheme (not to scale): (a) reflection mode, (b) transmission mode.

To ensure a physically accurate assessment of resolving power, it is essential to appropriately define the illumination conditions. In our calculations, we assume that the illumination is created by an incoherent light source focused onto the sample surface using a lens. In the reflection geometry, the light source is positioned above the sample, while in the transmission geometry, it is located below the sample.

Since the light source is assumed to be incoherent, the calculation is performed for individual beams focused to a half-wavelength spot, with the focal point gradually shifted along the sample surface. The resulting intensities are then summed. The focal shift area depends on the visualization mode. For reflection mode, this area should exceed the size of the microsphere so that further increasing the beam's spread does not alter the final image. In the presented calculations, this area ranged from  $-1.7R$  to  $1.7R$ , where  $R$  is the radius of the particle under investigation.

For the transmission geometry, the light only passes through the limited area of the apertures, so it suffices to simulate beams focused on the aperture region rather than the entire particle size. In these calculations, the focal shift area ranged from  $-2\lambda$  to  $2\lambda$ , where  $\lambda$  is the

wavelength. However, the step size of the focal shift must be particularly small, determined by the characteristic size of the apertures themselves. According to this scheme, the coherence radius in the substrate plane equals  $\lambda/2$ . Increasing the coherence radius can result in coherent effects, manifesting as a minor dip in the object image intensity in the absence of the microsphere [9]. Fig. 2 shows the near field and the corresponding image field in the absence of a microsphere at different distances between objects.

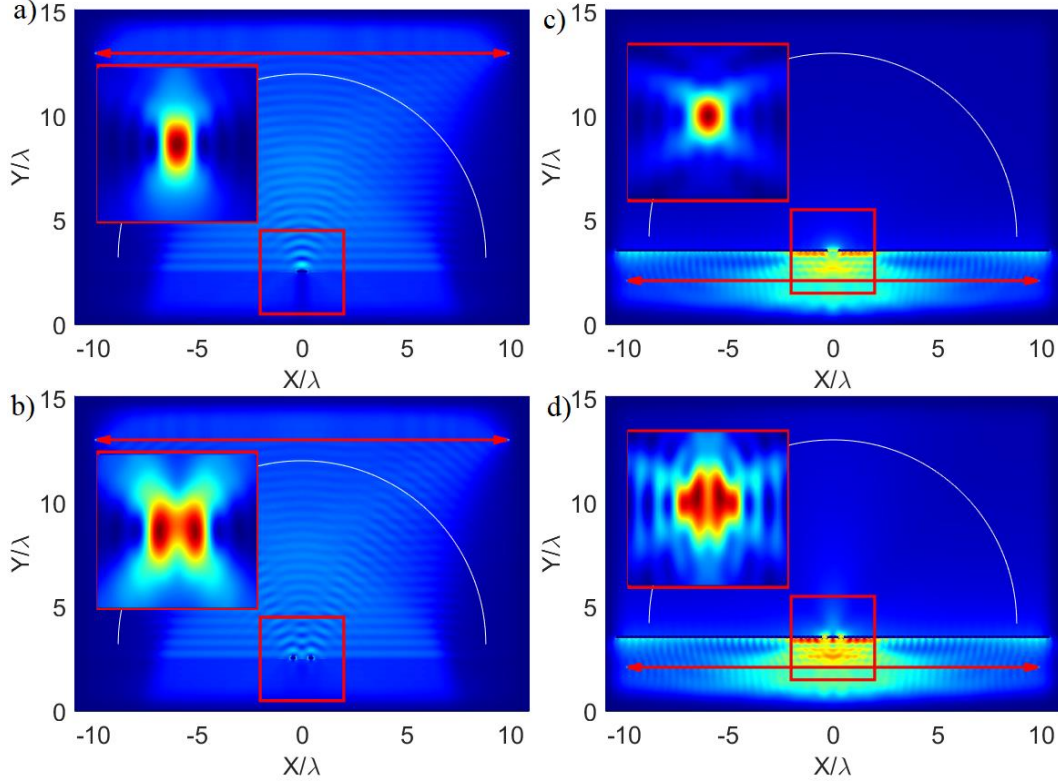


**Fig. 2.** Real fields without a microsphere and the corresponding image fields are shown in the insets. The white line represents the integration path  $\Gamma$ , while the double red arrow indicates the source generation line, the red double arrow line represents source injection line. The insets display the image field calculated for the area highlighted by the red square. (a, b) – Reflection mode, with distances between objects  $d=0$  and  $d=0.6$ , respectively. (c, d) – Transmission mode, with distances between apertures  $d=0$  and  $d=0.55$ , respectively.

### 3. Image formation algorithm and criterion of the resolution

To determine optical resolution, the calculation of the image field is performed at fixed object positions and particle radius. Analogous to FDTD calculations, the image field computation includes the following steps:

1. **Focused Beam Calculation:** A Gaussian beam tightly focused to  $\lambda/2$  on the sample plane is calculated.
2. **Beam Position Shift:** The focal point of the beam is shifted along the sample plane, and the calculation is repeated.
3. **Integration Across Incoherent Beam Width:** Calculations are performed across the chosen width of the incoherent beam by varying the focal position. The total intensity distribution is obtained by summing contributions from all focal positions.
4. **Image Field Calculation:** At each step, the image field is calculated, and the intensities from each focal position are summed to produce the final image.

The image field is computed using Eq. (1) in a rectangular area centered at the geometric image position, determined by the magnification formula  $n/(2-n)R$ , with dimensions approximately  $2R \times 2R$ .

Let the maximum of the image field distribution for  $x>0$  be at point  $A_1$ , and for  $x<0$  at point  $A_2$ . The objects are considered resolvable if:

- The intensity at the midpoint  $A_{12}$  has an 80% dip,
- The distance between points  $A_1$  and  $A_2$  is greater than the separation between objects,
- The  $y$ -coordinates of points  $A_1$  and  $A_2$  differ by no more than one wavelength.

Conditions (b) and (c) are not strictly necessary but serve as checks for accuracy in the calculations. In many cases, due to overlapping image fields from each object, the maximum shifts toward the center above or below two distinct local maxima. If this central maximum is excluded, conditions (a)-(c) are satisfied, and the objects (e.g., slits) can be considered resolvable. However, such cases are excluded from the presented calculation, meaning that the optical resolution is estimated conservatively, or “from below”.

The first calculation is performed with zero separation between slits. In some cases, conditions (a)-(c) are satisfied even with zero separation, indicating that the sphere does not form an image that defines the object's geometry, and the resolution is considered indeterminate. The calculation then proceeds to the next particle size. If the slits are not distinguishable in the image field, their separation is increased by  $0.05\lambda$ , and the calculation is repeated until conditions (a)-(c) are met. Fig. 3 shows the near fields and image fields in the presence of a microparticle at different distances, when objects are distinguishable and indistinguishable.

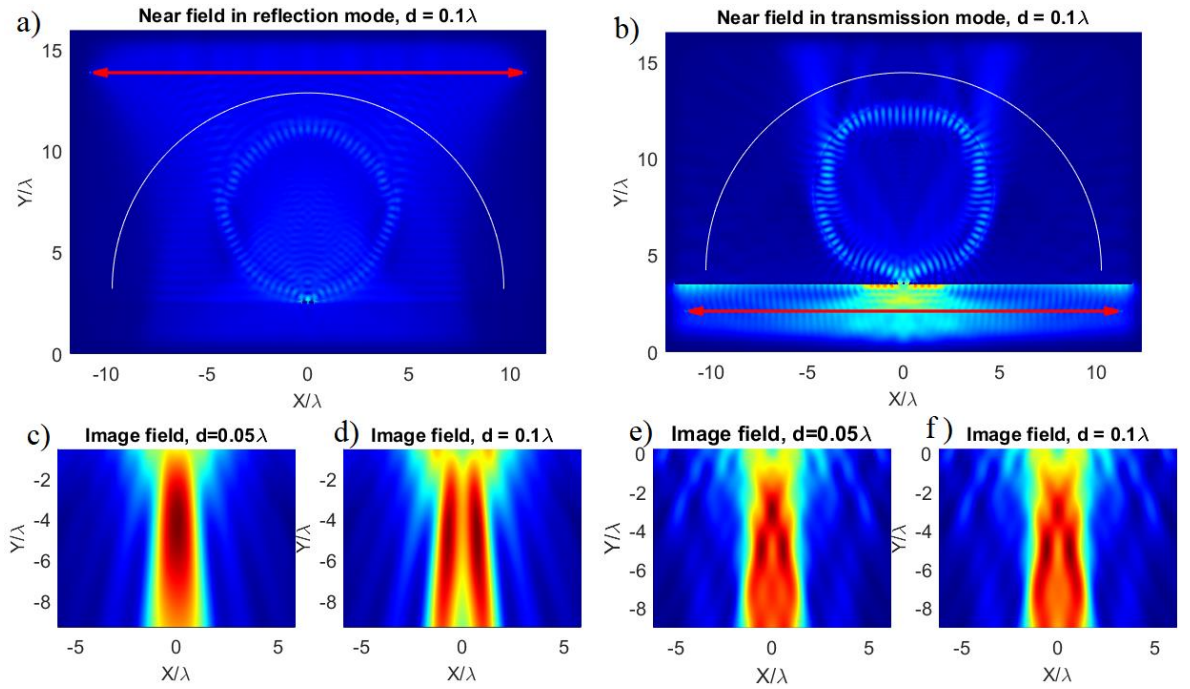


**Fig. 3.** (a, b) Near-field distribution in reflection and transmission modes, respectively. Image field in reflection mode with object separation of  $d=0.05\lambda$  – (c),  $d=0.1\lambda$  – (d). Image field in transmission mode with slit separation of  $d=0.05\lambda$  – (e),  $d=0.1\lambda$ – (f). The particle radius in reflection mode is  $R=4.4\lambda$ , and in transmission mode,  $R=4.66\lambda$ . The white line represents the integration path  $\Gamma$ , while the double red arrow indicates the source generation line, the red double arrow line represents source injection line.

## 4. Results

In Fig. 4, the graph illustrates the dependence of optical resolution on the size of the microparticle in transmission mode (TM) and reflection mode (RM). Fig. 4 also shows the resolution in free space, which slightly differs from  $\lambda/2$  and is approximately  $0.6\lambda$ . This can be explained by two factors: (a) the objects are not point sources, and (b) the coherence radius is not zero. The resolution

in transmission mode is somewhat lower than in reflection mode. This is due to the light being focused within the substrate, allowing it to be localized on a smaller scale. In the case where the substrate is removed but the conductor is present, the resolution in both modes equals  $0.6\lambda$ .

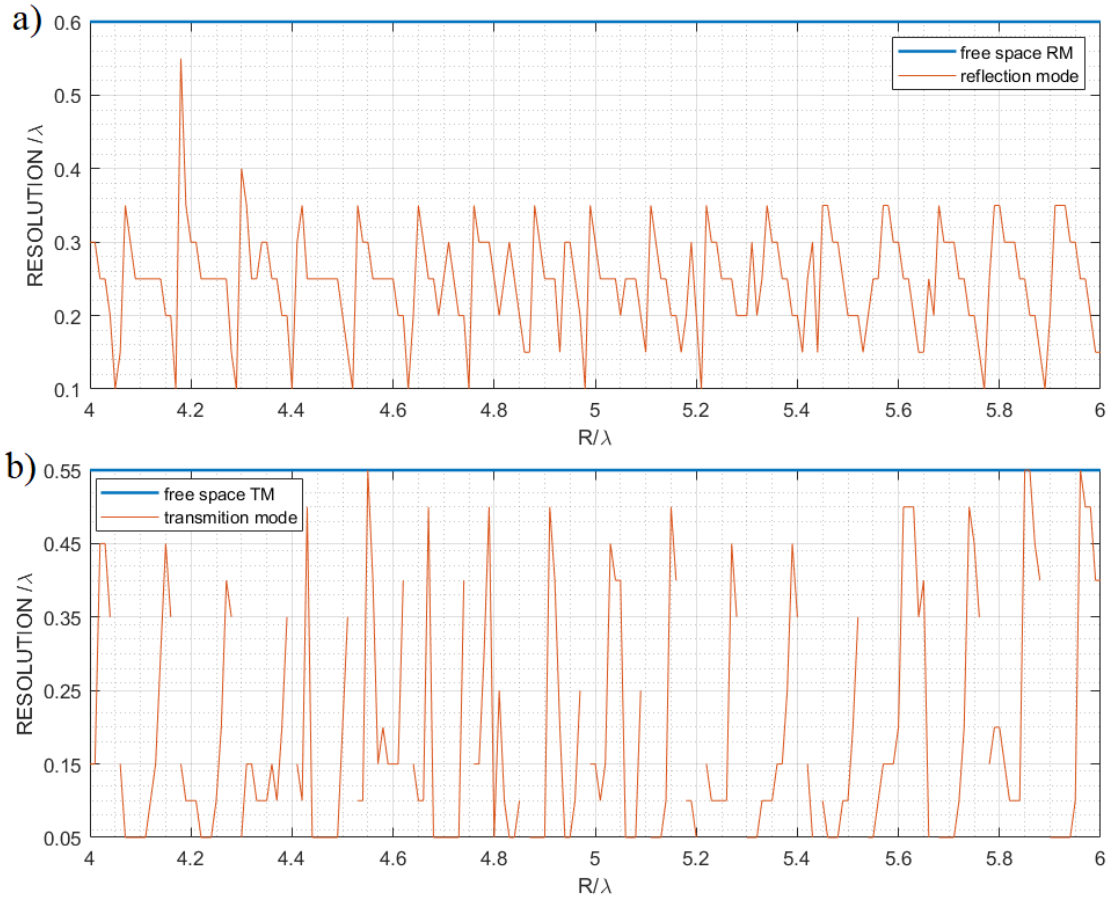


**Fig. 4.** Dependence of the optical resolution in the virtual image on the size of the microparticle: reflection mode – (a), transmission mode – (b). The blue solid lines indicate the resolution in free space without the microparticle. At the discontinuity points in the graph for the transmission mode, the resolution is undefined because the slits are distinguishable (i.e., formal conditions a)-c) are satisfied) at zero distance.

The calculations showed that the resolution in free space, i.e., in the real image, is approximately the same for both reflection and transmission geometries, while for the imaginary image, i.e., when a microparticle is present, it differs significantly. However, in all cases, the optical resolution exceeds the limit in free space.

Let's take a closer look at the break points on the graph in Fig. 4. As mentioned earlier, these breaks occur because the conditions a)–c) are met when the distance between the slits is zero, which represents a kind of contradiction. Let's examine this case in more detail, using the break point at  $R/\lambda = 4.4$  as an example. In this case, the resolution is given an undefined value. At first glance, it might seem that the conditions a)–c) would continue to be valid as the slit distance increases, but this is not the case. If we calculate with a distance of  $d = 0.1\lambda$ , these conditions are no longer met, and this trend persists up to a distance of  $d = 0.25\lambda$ , a value that can be obtained by interpolation from the graph. Thus, this can be considered, with some reservations, the optical resolution in this case. Fig. 5 illustrates this behavior in more detail. However, in the illustrated example, this rule can be violated, which indicates the need for the development of more general criteria for optical image resolution.

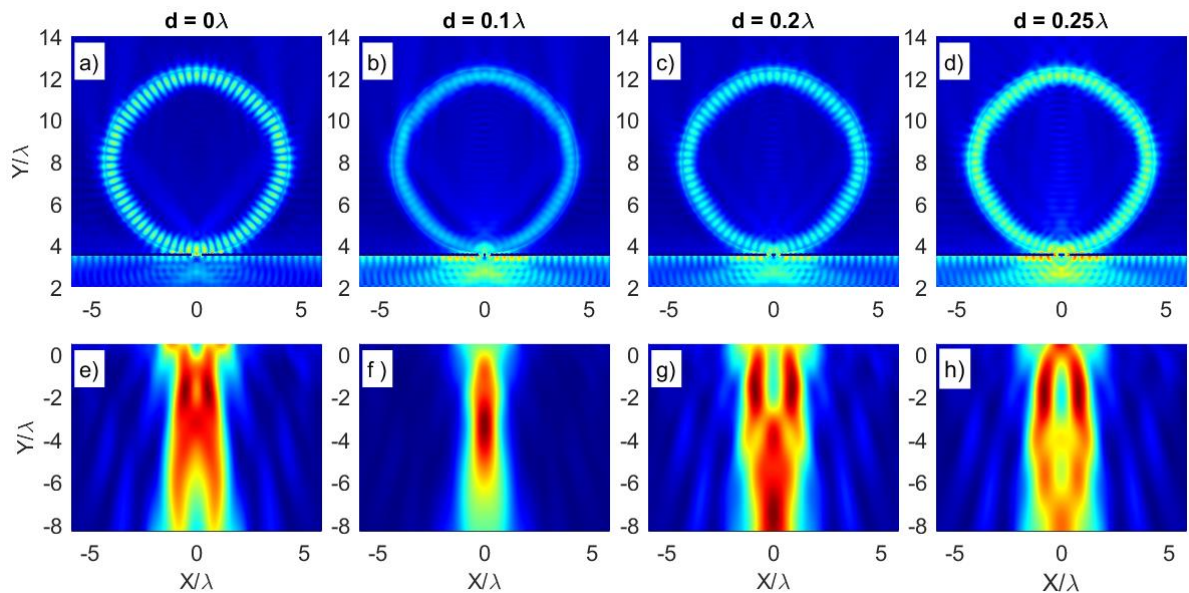


**Fig. 5.** (a, b, c, d) - Near-field distribution near the slits for  $R = 4.4\lambda$ , corresponding to the break points in Fig. 44, with slit distances  $d/\lambda = 0, 0.1, 0.2, 0.25$ , respectively. (e, f, g, h) - Image fields corresponding to the cases shown in the images above. Formal conditions for distinguishability are satisfied at  $d/\lambda = 0$ , however, in reality, the slits are distinguishable only at  $d/\lambda = 0.25$ .

## References

1. H. Yang, R. Trouillon, G. Huszka, *et al.*, "Super-resolution imaging of a dielectric microsphere is governed by the waist of its photonic nanojet," *Nano Lett.*, **16**(8), 4862-4870 (2016).
2. R. Boudoukha, S. Perrin, A. Demagh, *et al.*, "Near-to far-field coupling of evanescent waves by glass microspheres," *Photonics*, **8**(73), 59 (2021).
3. Y. Duan, G. Barbastathis, and B. Zhang, "Classical imaging theory of a microlens with super-resolution," *Opt. Lett.* **38**(16), 2988-2990 (2013).
4. A. Bekirov, B. Luk'yanchuk, and A. Fedyanin, "Virtual image within a transparent dielectric sphere," *JETP Lett.* **112**(6), 341-345 (2020).
5. T. Pahl, L. Hüser, S. Hagemeyer, *et al.*, "FEM-based modeling of microsphere-enhanced interferometry," *Light adv. manuf.* **3**(4), 699-711 (2022).
6. C. Simovski, and H. Reza, "A simple glass microsphere may put the end to the metamaterial superlens story," *AIP Conf. Proc.* **2300**, 020117 (2020).
7. V. Astratov, Y. Sahel, Y. Eldar, *et al.*, "Roadmap on Label-Free Super-Resolution Imaging," *Laser Photonics Rev.* **17**(12), 2200029 (2023).
8. A. Maslov, "Effect of boundary conditions in modeling of microsphere-assisted imaging," *Appl. Opt.* **63**(16) 4372-4379 (2024).
9. A. Maslov, and V. Astratov, "Origin of the super-resolution of microsphere-assisted imaging," *Appl. Phys. Lett.* **124**(6), 061105 (2024).
10. S. Lee, L. Li, Y. Ben-Aryeh, *et al.*, "Overcoming the diffraction limit induced by microsphere optical nanoscopy," *J. Opt.* **15**(12), 125710 (2013).
11. A. Bekirov, "On superresolution in virtual image in a transparent dielectric sphere," *Opt. Spectrosc.* **131**(3), 363-369 (2023).
12. A. Bekirov, B. Luk'yanchuk, Z. Wang, *et al.*, "Wave theory of virtual image," *Opt. Mater. Express* **11**(11), 3646-3655 (2021).
13. Bekirov, A. R., Wang, Z., Luk'yanchuk, B. S., & Fedyanin, A. A. (2024). Dielectric microparticles for enhanced optical imaging: an FDTD analysis of contrast and resolution. *Journal of the Optical Society of America A*, **42**(1), 45-50
14. Allen, Kenneth W., *et al.* "Overcoming the diffraction limit of imaging nanoplasmonic arrays by microspheres and microfibers." *Optics express* **23.19** (2015): 24484-24496.